Journal of Colloid and Interface Science 605 (2022) 674–684

Contents lists available at ScienceDirect

Journal of Colloid and Interface Science

journal homepage: www.elsevier.com/locate/jcis

Rare-earth single atoms decorated 2D-TiO_2 nanosheets for the photodegradation of gaseous O-xylene

Junfeng Chen [a,b], Lu Chen [b], Xiao Wang [b], Zepeng Rao [b], Jing Sun [b], Aiying Chen [a,*], Xiaofeng Xie [b,*]

[a] University of Shanghai for Science and Technology, 516 Jungong Road, Shanghai 200093, China
[b] State Key Lab of High Performance Ceramics and Superfine Microstructure, Shanghai Institute of Ceramics, Chinese Academy of Sciences, 1295 Dingxi Road, Shanghai 200050, China

HIGHLIGHTS

- The decreased adsorption energy of TiO_2 decorated with rare-earth single atoms enhanced the adsorption capability to O-xylene.
- Improved charge separation was ascribed to charge transfer channel between rare-earth atom and O atom.
- TiO_2 decorated with rare-earth single-atom exhibited an enhanced photocatalytic performance.
- The influence of rare-earth single atoms on intermediates produced of O-xylene during photocatalytic process was proposed.

GRAPHICAL ABSTRACT

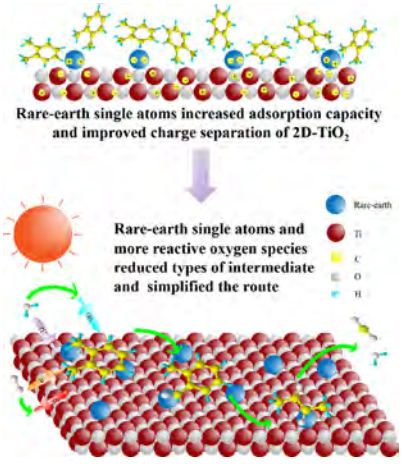

ARTICLE INFO

Article history:
Received 20 June 2021
Revised 22 July 2021
Accepted 25 July 2021
Available online 29 July 2021

Keywords:
Single atoms
Rare-earth
2D-TiO_2
Photocatalytic oxidation
O-xylene

ABSTRACT

In this work, rare-earth single atoms (La, Er) were decorated on the surface of 2D-TiO_2 nanosheets by an impregnation-calcination strategy. The formation of rare-earth single atoms was certified by AC HAADF-STEM and XAS. TiO_2 decorated with rare-earth single atoms (La_1-TiO_2 and Er_1-TiO_2) exhibited outstanding photocatalytic activity than pure 2D-TiO_2 nanosheets (2D-TiO_2) towards gas-phase degradation of O-xylene. Compared with 2D-TiO_2, the rare-earth single atoms greatly improved the adsorption capacity of O-xylene without increasing their specific surface area. This is because rare-earth single atoms provide additional adsorption sites and reduce the adsorption energy of O-xylene. In addition, the hybrid orbital formed by the combination of rare-earth single atom and oxygen atom is beneficial to the rapid transmission and separation of photo-induced electrons, thereby improving the performance of photocatalytic degradation. In addition, *in-situ* DRIFTS and GC–MS were used to reveal the photocatalytic oxidation mechanism. Interestingly, the results showed that the La_1-TiO_2 and Er_1-TiO_2 samples can reduce the types of intermediates and simplify the reaction route, implying that the single atoms play an important role in the modulation and thorough mineralization of intermediate products. This work shows that the rare-earth single atom decorated 2D-TiO_2 nanosheets have great potential in photocatalytic air pollution control.

* Corresponding authors.
E-mail address: aychen@usst.edu.cn (A. Chen).

https://doi.org/10.1016/j.jcis.2021.07.129
0021-9797/

1. Introduction

Volatile organic compounds (VOCs) emitted to the atmosphere should be handled, which not only pollute the living environment, but also do harm to the human health [1–4]. Compared with adsorption [5], plasma treatment [6] and thermal catalysis [7], photocatalysis technology is an environmentally friendly treatment, which directly uses sunlight to produce electrons and holes, and then electrons and holes produce reactive oxygen species to achieve efficient removal of VOCs [8]. TiO_2 is the most commonly used photocatalyst due to its chemical stability, non-toxic and low cost [9,10]. However, there are still some problems, such as limited active sites and rapid recombination of photo-induced e^--h^+ pairs, limiting their practical application for removing VOCs. Researchers have made a lot of efforts to modify TiO_2, including doping with metallic elements [11] or nonmetallic elements [12]. noble metal loading [13] and incorporating with two-dimensional materials [14] or other semiconductors [15]. In addition, TiO_2 is promising support for single atoms, especially 2D-TiO_2 nanosheets, which with abundant surface defects can facilitate the loading and dispersion of single atoms on its surface [16].

Due to high catalytic activity, good selectivity and maximum atomic availability, semiconductor decorated with single atoms has become a new method to improve the catalytic performance [17]. Researchers focused on noble metal elements at first, such as Pt [18], Au [19], Ru [20] and Ag [21]. And then researchers noticed that transition metal elements are potential, like Fe [22], Co [23], Ni [24] and Cu [25]. Owing to unique electronic, optical and magnetic properties, the rare-earth elements have been studied and used in a variety of fields. As for photocatalysis, different rare-earth ions have been used as dopants in TiO_2 to improve the photodegradation performance of TiO_2 in liquid-phase [26] and gas-phase [11,27]. After doped with rare-earth ions, an upconversion phenomenon occurred and impurity states (RE-4f level) were introduced. However, it's unclear what will happen when rare-earth dispersed atomically on semiconductor supporter. In addition, as a scarce resource, it should be used more reasonably and more efficiently. There is no doubt that it is of practical significance to study the properties of rare-earth elements on the atomic scale. Some researches about rare-earth elements at a single atom scale have been reported in photocatalytic CO_2 reduction and other fields. Y and Sc single atoms with catalytic activities to N_2 reduction reaction and CO_2 reduction reaction were successfully synthesized on a carbon support while Y_2O_3 and Sc_2O_3 nanoparticles were generally inactive to those reactions [28]. A novel and universally applicable atom-confinement and coordination strategy was reported by Ji et al. [29] to achieve the synthesis of rare-earth single atoms supported on carbon nitride nanotubes which exhibited excellent photocatalytic CO_2 reduction reaction performance. Chen et al. [30] also reported a method to achieve the synthesis of rare-earth La single atoms supported on carbon nitride and revealed the function of the charge-transfer bridge formed between La atom and N atom. However, rare-earth single atoms were still rarely studied. Especially, exploration of rare-earth single atoms on TiO_2 photocatalyst and their related mechanisms of photocatalytic removal of VOCs have been seldom reported yet. In addition, the above pyrolysis syntheses had disadvantages such as long preparation cycles or requiring high or low temperature treatment. Therefore, it's meaningful to develop a relatively mild preparation process to combine rare-earth single atoms with TiO_2 in order to use rare-earth resources more efficiently and investigate the key role of rare-earth single atoms in the enhancement of photocatalytic oxidation activity for VOCs and the modulation of intermediates.

In this work, we successfully fabricated the rare-earth Er single atoms and La single atoms decorated TiO_2 by a facile impregnation-calcination strategy. Compared with pure 2D-TiO_2, single atoms Er and La decorated TiO_2 exhibited improved adsorption capacity and higher charge separation ability, attributing to large size rare-earth atoms with high coordination numbers causing an unusual coordination environment. The synergistic effect of improved adsorption capacity and higher charge separation ability enhanced the photocatalytic degradation of O-xylene. The degradation routes of gaseous O-xylene were studied by *in-situ* DRIFT and GC–MS. And the detected intermediates indicated that O-xylene degraded through different routes on 2D-TiO_2 and TiO_2 decorated with rare-earth single atoms. In this work, we got a preliminary understanding of the role of rare-earth single atoms played in photocatalytic oxidation of O-xylene and provided an idea that using rare-earth single atoms to degrade other VOCs.

2. Experimental

2.1. Chemicals

Tetrabutyl titanate, Hydrofluoric acid and $La(NO_3)_3{\cdot}nH_2O$ were purchased from Sinopharm Chemical Reagent Co., Ltd. $Er(NO_3)_3{\cdot}6H_2O$ was purchased from Sigma-Aldrich. Absolute ethanol as solvent was purchased from Zhenxing Co., Ltd. All chemicals used in our research were used without any further purification.

2.2. Synthesis of 2D-TiO_2 nanosheets

2D-TiO_2 nanosheets were synthesized via a solvothermal method[10]. Briefly, 6 mL hydrofluoric acid (40%) was added to 50 mL titanium (IV) isopropoxide (TIP) dropwise under magnetic stirring and kept under stirring for 2 h. After being transferred into a 100 mL Teflon-lined autoclave, the solution was heated at 180 °C for 36 h. Next, the precipitate cooled to room temperature and was separated by centrifugation. After that, the precipitate was washed with absolute ethanol and deionized water for three times, respectively. Next, the powders were dispersed in 100 mL 0.1 M NaOH aqueous solution and stirred for 8 h. Then, the sample was separated by centrifugation and washed with absolute ethanol and deionized water for three times. Finally, the powder obtained was dried at 80 ℃ for 6 h. The obtained samples were noted as 2D-TiO_2.

2.3. Synthesis of rare-earth single atoms decorated TiO_2

The obtained 2D-TiO_2 were transferred to a tube furnace and calcined at 250 °C for 2 h in a reductive atmosphere (5 vol% hydrogen and 95 vol% argon) to introduce oxygen vacancies on the surface of TiO_2.

0.5 g 2D-TiO_2 with oxygen vacancies were dispersed in 50 mL absolute ethanol followed by ultrasounding for 1 h. Then, 10 mL absolute ethanol with about 0.0069 g $Er(NO_3)_3{\cdot}6H_2O$ was added under magnetic stirring and kept under stirring for 12 h. Next, the precipitate was separated by centrifugation and then washed with deionized water for three times. After drying at 80 ℃ for 4 h, the obtained powder was transferred to a tube furnace and calcined at 200 °C for 2 h in a reductive atmosphere (5 vol% hydrogen and 95 vol% argon) to form rare-earth Er single atoms on the surface. The obtained samples were noted as Er_1-TiO_2.

Rare-earth La single atoms decorated TiO_2 was synthesized by following the similar procedures except that $Er(NO_3)_3{\cdot}6H_2O$ was

replaced by $La(NO_3)_3{\cdot}nH_2O$. The obtained sample was noted as La_1-TiO_2.

2.4. Characterization

The crystal structures of the samples were measured by X-ray diffraction (XRD) equipped with a high-resolution powder X-ray diffractometer (D8 ADVANCE) using Cu Ka radiation (λ = 0.15418 nm, 2θ varied from 10° to 80°, 5°/min). Raman spectra were collected on a DXR spectrometer (Thermal Scientific Corporation, USA) under the excitation of laser wavelength λ_{ex} = 532 nm with laser power of 8 mW. The BET specific surface area (S_{BET}) was measured by Micromeritics ASAP 3000. X-ray absorption spectra (XAS) including X-ray absorption near-edge structure (XANES) and extended X-ray absorption fine structure (EXAFS) were acquired by Shanghai Synchrotron Radiation Facility (SSRF). The morphologies and microstructures of samples were observed by field-emission scanning electron microscope (FE-SEM, Magellan 400), field-emission transmission electron microscope (JEM-2100F) and transmission electron microscopy with spherical aberration correction for condenser lens (Hitachi-HF5000). Temperature-programmed desorption (TPD) was performed on a chemisorption analyzer (PCA-1200). UV–vis diffuse reflectance spectra were obtained by using an ultraviolet spectrophotometer (Cary 5000). Photoluminescence spectra were performed on a luminescence spectrometer 55 (LS55, Perkin-Elmer) with an excitation wavelength of 250 nm. ESR spectra were obtained by a JES-FA200 spectrometer. *In-situ* diffuse reflectance infrared Fourier transform spectroscopy (*In-situ* DRIFT) analysis was performed on a spectrometer (IRTracer-100, Shimadzu). Intermediates were detected by gas chromatography-mass spectrometer (GCMS-QP2010Ultra, Shimadzu).

2.5. Adsorption capacity and photocatalytic activity

First, we immobilized the sample on a glass plate (12 * 5 cm). Typically, 105 mg sample was dispersed in about 10 mL absolute ethanol into the mortar and was coated on a glass plate after grinding for 10 min. The adsorption capacity and photocatalytic activity of O-xylene were measured by a test system for continuous flow of gas which was equipped with a gas mixer, reaction chamber and gas chromatograph [11]. After drying at room temperature, the above glass plate coated with sample (100 mg) was placed in the reaction chamber and sealed tightly. And then 50 ppm O-xylene and air were mixed in a gas mixer and flowed through the reaction chamber. After achieving an adsorption–desorption equilibrium in dark, the xenon lamp (400 W) was turned on. The distance between the light source and the surface of the sample was 30 cm.

The adsorption capacity (A_c) of O-xylene was calculated by the Eq. (1):

$$Ac = \{C_0 \times \rho 1 \times \rho 2 \times [\int_0^t v \times (1 - C/C_0)dt]\text{sample} - [\int_0^t v \times (1 - C/C_0)dt]\text{blank}\}/(M \times m) \quad (1)$$

The degradation efficiency (x) of o-xylene was calculated by the Eq. (2):

$$x = (1 - C/C_0) \times 100\% \quad (2)$$

ρ_1 and ρ_2 represent the air density and the relative vapor density of VOC, respectively; v represents the flowing speed of O-xylene; C_0 is the initial concentration of O-xylene; $C$is the real-time concentration of O-xylene; M and m represent the molar mass of o-xylene and photocatalyst mass, respectively.

3. Results and discussion

3.1. Characterization of photocatalysts

The crystal structures of the as-prepared samples were characterized by XRD. As shown in Fig. 1a, 2D-TiO_2 displayed characteristic peaks located at 25.1°, 46.4° and 55.1°, ascribed to anatase phase TiO_2, which confirmed that the as-prepared TiO_2 was pure anatase phase [31]. Comparing with pure 2D-TiO_2, no new characteristic peaks were observed in the Er_1-TiO_2 and La_1-TiO_2, which implied that few or even no rare-earth oxides existed and the loaded rare-earth metals were very likely to exist as single atoms on 2D-TiO_2. Four characteristic peaks (143, 393, 513 and 635 cm^{-1}) were observed in Raman spectra (Fig. 1b), giving a further evidence that the samples were anatase phase TiO_2 [32]. If there were rare-earth oxides loaded on 2D-TiO_2, residual stress appeared and led to the shift of Raman peaks [33]. However, no blue shift or red shift was observed in Raman spectra, further indicating that rare-earth elements may exist in the form of single atoms, which was consistent well with mentioned XRD results.

The morphology of 2D-TiO_2 was flake-like in Fig. 2c. And the BET specific surface area of 2D-TiO_2, Er_1-TiO_2 and La_1-TiO_2 were 65.52 m^2/g, 68.27 m^2/g and 69.09 m^2/g, respectively in Table 1. As shown in TEM of Er_1-TiO_2 (Fig. 2a) and La_1-TiO_2 (Fig. 2b), the size of nanosheets was about 30–50 nm and the thickness was

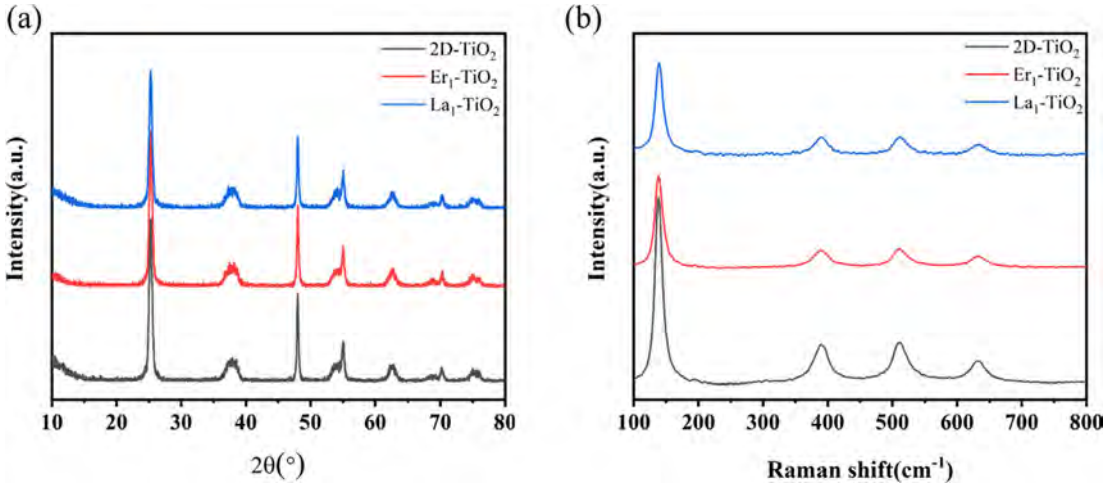

Fig. 1. (a) XRD and (b) Raman spectra of 2D-TiO_2, Er_1-TiO_2 and La_1-TiO_2.

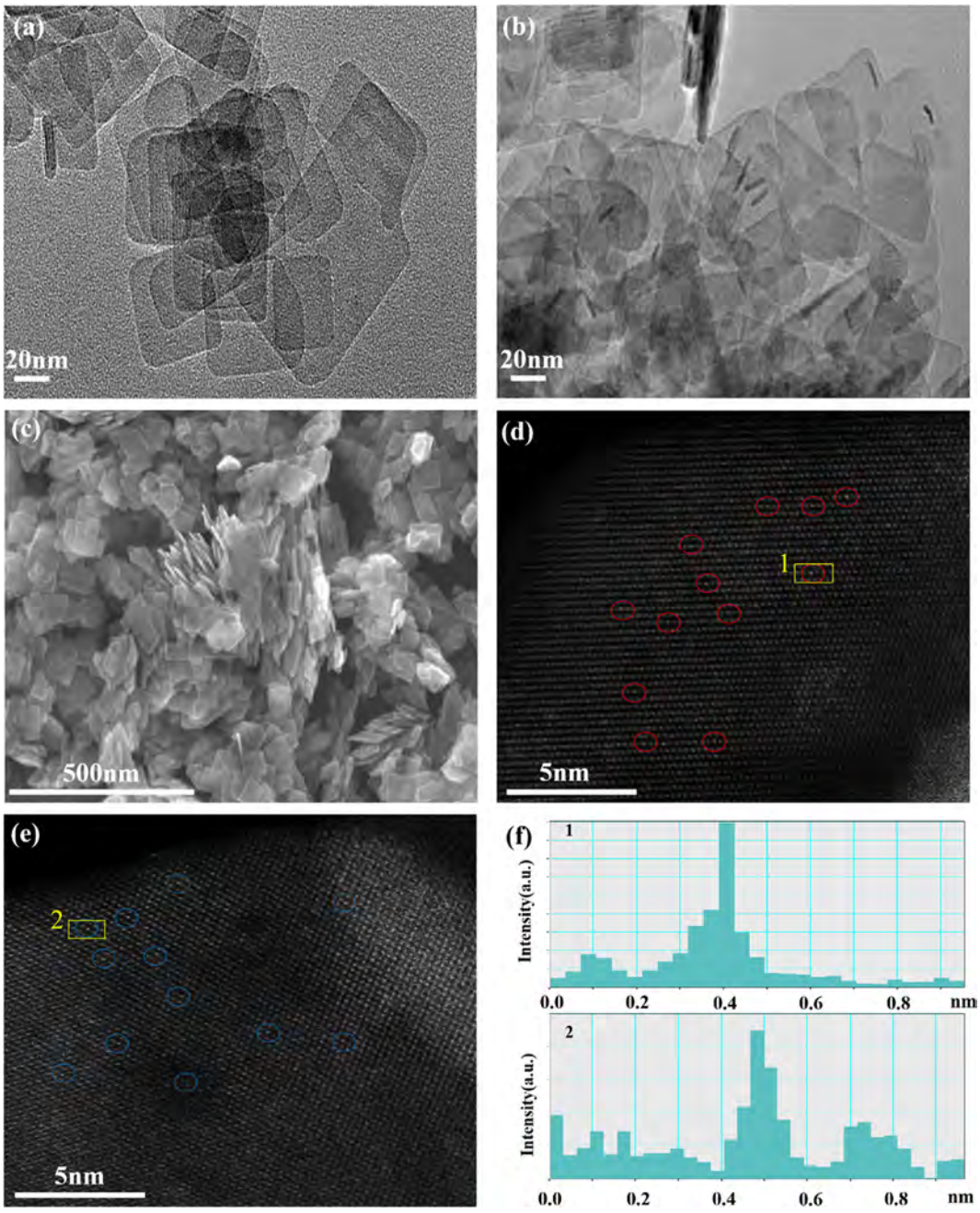

Fig. 2. TEM images of (a) Er_1-TiO_2, (b) La_1-TiO_2; (c) SEM image of 2D-TiO_2; AC HAADF-STEM images of (d) Er_1-TiO_2, (e) La_1-TiO_2; (f) line-scanning intensity profiles obtained in (d) and (e).

Table 1
The BET specific surface area of the as-prepared samples.

Sample	2D-TiO_2	Er_1-TiO_2	La_1-TiO_2
S_{BET} (m^2/g)	65.52	68.27	69.09

about 6–8 nm, and there were no obvious nanoparticles observed, while no obvious nanoparticles or clusters were found through transmission electron microscopy with spherical aberration correction (HAADF-STEM), excluding the formation of rare-earth oxides or clusters. And bright dots highlighted by circles can be obviously observed in Fig. 2d and Fig. 2e, corresponding to atomically dispersed rare-earth metals. Only one maximum peak was observed in line-scanning intensity profiles (Fig. 2f), which was ascribed to rare-earth atom [34].

The coordination environment and electronic structure of the Er atoms supported on 2D-TiO_2 were investigated by XAFS including EXAFS and XANES. The k_3-weighted EXAFS at the Er L_{III} edge for the Er_1-TiO_2 and Er_2O_3 in R space were shown in Fig. 3a. As for Er_2O_3, peaks located around at 1.79 Å and 3.48 Å ascribed to Er-O coordination and Er-Er coordination, respectively. Different from Er_2O_3, no peak at around 3.48 Å assigned to Er-Er coordination was observed in Er_1-TiO_2. The results obtained by EXAFS were further confirmed by wavelet transform analysis (Fig. 3b). Er_2O_3 had two intensity maximum, one at about 4.5 $Å^{-1}$ and another at about 7 $Å^{-1}$, corresponding to Er-O bonding and Er-Er bonding, respectively. Er_1-TiO_2 only had one intensity maximum at about 3 $Å^{-1}$ ascribed to Er-O bonding. The results of EXAFS and wavelet transform analysis indicated jointly that Er atoms in Er_1-TiO_2 neither

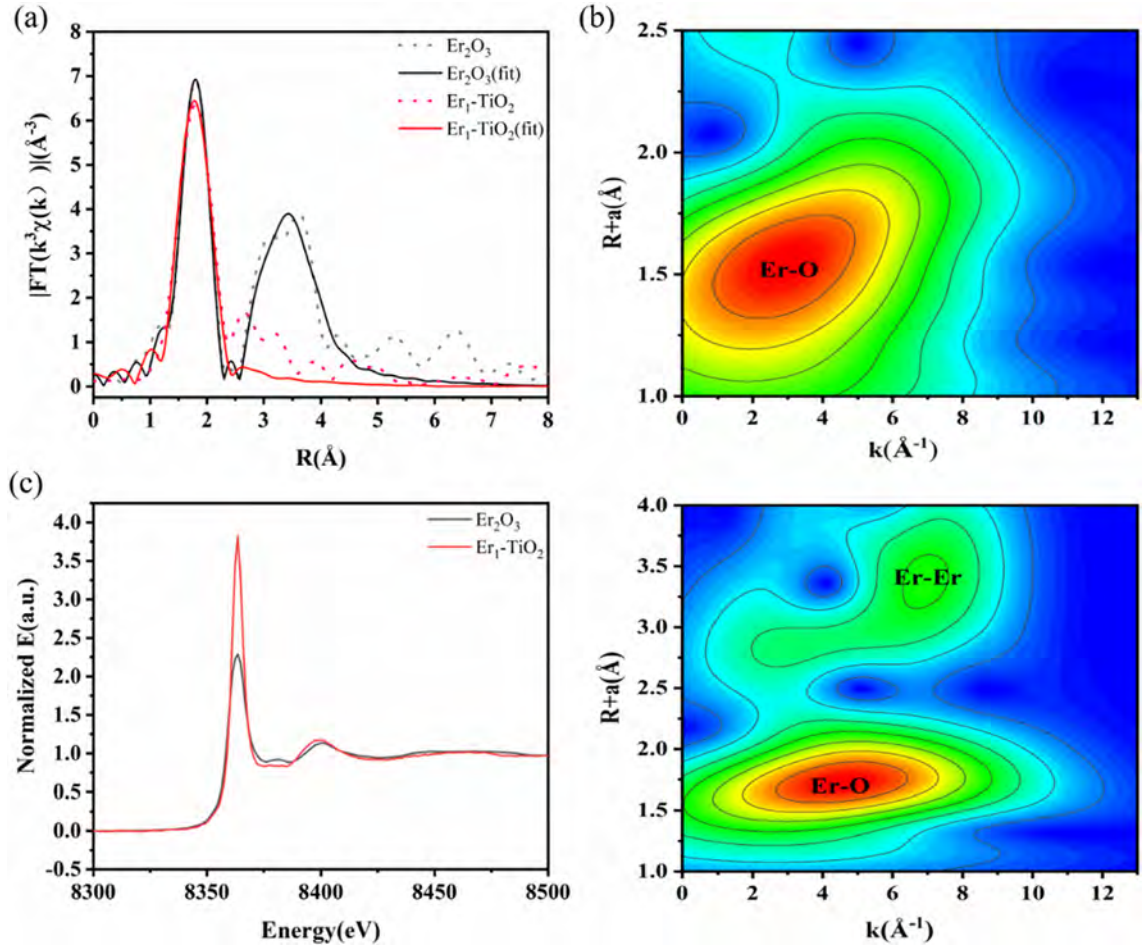

Fig. 3. (a) Er L_3-edge k^3-weighted Fourier transform (FT) spectra of the Er_1-TiO_2 and Er_2O_3 samples; (b) Wavelet transform (WT) of the Er_1-TiO_2 and Er_2O_3 samples; (c) Er L_3-edge XANES spectra of the Er_1-TiO_2 and Er_2O_3 samples.

Table 2
EXAFS fitting parameters at the Cu K-edge various samples(S_0^2 = 0.82).

Sample	Path	C.N.	R (Å)	$\sigma^2 \times 10^3$(Å^2)	ΔE (eV)	R factor
	Er-O	6	2.25 ± 0.01	7.4 ± 1.8	0.4 ± 1.4	0.018
Er_2O_3	Er-Er	3	3.43 ± 0.04	4.4 ± 1.9	−6.2 ± 4.3	0.018
	Er-Er	3	3.91 ± 0.04	1.9 ± 1.8	−6.2 ± 4.3	0.018
Er_1-TiO_2	Er-O	7.4 ± 1.1	2.28 ± 0.01	9.3 ± 2.4	0.3 ± 1.2	0.007

formed oxides nor crystallized into crystalline structures. Er atoms in Er_1-TiO_2 existed as single atoms, consistent well with the result of HAADF-STEM. Quantitative least-squares fitting parameters of EXAFS were shown in Table 2. The fitting results indicated that one Er atom was coordinated with about seven O atoms, and the average Er-O bond length was 2.28 Å. Different from other metal atom, Er atom with relatively larger size had relatively higher coordination numbers. The valence state of the element can be revealed by X-ray absorption near edges structure (Fig. 3c). Compared with Er_2O_3, Er_1-TiO_2 exhibited increased white-line intensity, indicating that the valence state of Er was higher than + 3. XANES results suggested that there was a strong interaction between Er atom and O atoms coordinated, leading to charge transfer between two kinds of atoms and Er atom acted as electron-donor.

3.2. Influence factors of photocatalysis

According to the above results, we draw a conclusion that rare-earth single atoms were supported on 2D-TiO_2 successfully. The presence of single atoms has some effects on the properties of 2D-TiO_2. There are some factors which will affect the photocatalytic activity of catalysts, such as adsorption capacity, light absorption ability and charge separation ability.

During the whole photocatalytic reaction process, the pollutant adsorption reaction takes place at first, and then the next reaction follows. Thus, adsorption capacity is one of the important factors. As shown by the dynamic dark adsorption curve (Fig. 4a), the maximum adsorption percentage of Er_1-TiO_2 reached 80% and those of La_1-TiO_2 reached 90%, while those of TiO_2 only reached 50%. And the adsorption capacity of La_1-TiO_2 was 1.5 times higher than that of 2D-TiO_2. Obviously, the presence of rare-earth single atoms improved the adsorption capacity of TiO_2. The results of TPD (Fig. 4b) was consistent with the results of dynamic adsorption. The intensity of the desorption peak of TiO_2 decorated with rare-earth single atoms was higher than that of TiO_2, suggesting that more O-xylene molecules were adsorbed. The desorption peak of La_1-TiO_2 located at around 150 ℃ was related to physical absorption and that located at around 300 ℃ was ascribed to chemical

adsorption, while Er_1-TiO_2 and TiO_2 only had a desorption peak located at around 300 ℃ which was related to chemical adsorption. The similar desorption temperature meant single atoms did not affect the adsorption configuration of the O-xylene molecules, while different desorption temperature may mean different adsorption configuration [35]. After decorated with single atoms, the specific surface area of samples increased slightly, which indicated that specific surface area had little contribution to the adsorption capacity. Due to the special coordination environment, the single atom became an additional adsorption active site to reduce the adsorption energy and thus increased the adsorption capacity [22,30].

Since it can only react under the excitation of light, the light absorption ability of photocatalysts is another important factor. As shown in the UV–visible spectrum (Fig. 5a), there was not much difference between pure 2D-TiO_2 and TiO_2 decorated with rare-earth single atoms. Compared with 2D-TiO_2, the light absorption ability of TiO_2 decorated with rare-earth single atoms increased slightly in the visible light region. Interestingly, Er^{3+}-doped TiO_2 had the upconversion phenomenon which could be ascribed to f-f electronic transitions of Er^{3+} [11] while TiO_2 decorated with Er single atoms did not. The reason why TiO_2 decorated with Er single atoms did not have the upconversion phenomenon may be that the difference in the electronic structure between Er atoms and Er^{3+} ions may result in the different electronic transition patterns when excited.

Charge separation ability is also an important factor. When excited by light, the photocatalysts form photo-generated carriers. And only when they are effectively separated can they take part in further photocatalytic reactions. Photoluminescence (PL) spectra can reveal the charge separation ability. As shown in Fig. 5b, the intensity of PL spectra for the photocatalysts decreased after the introduction of single atoms, which meant that charge separation ability improved and the recombination rate of photo-generated carriers decreased. The result of EXAFS indicated that Er atoms were coordinated with oxygen atoms. And the result of XANES demonstrated that the valence state of Er_1 was higher than Er^{3+}. The results of EXAFS and XANES suggested that Er atom had a strong interaction with the surrounding oxygen atoms, which may cause orbital hybridization of Er and O atoms [30]. This orbital hybridization facilitated the transfer of electrons from Er atoms to O atoms to form a charge transfer channel which resulted in the improvement of charge separation ability.

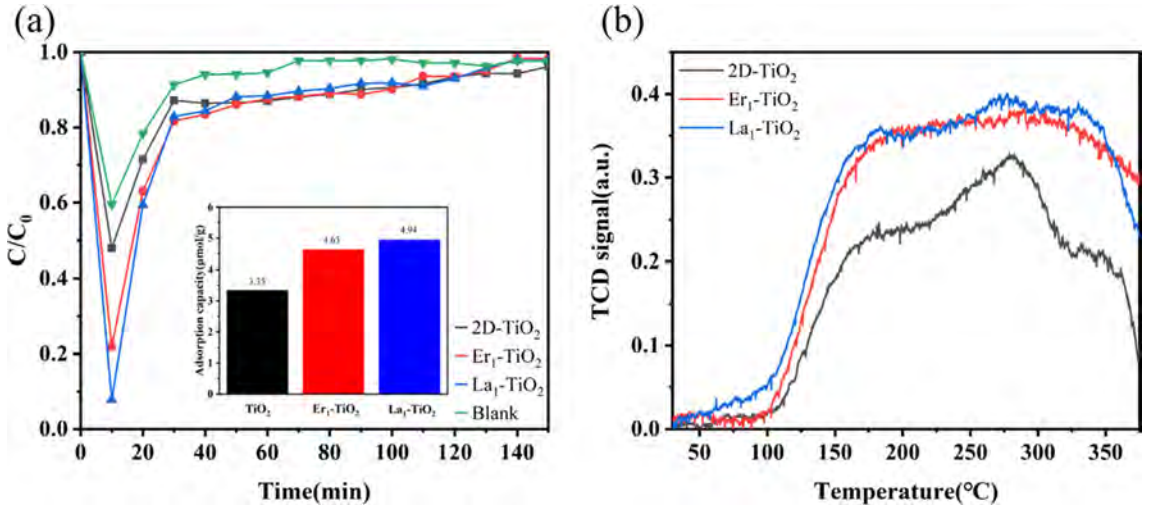

Fig. 4. (a) Dynamic adsorption plots of O-xylene and (b) temperature-programmed desorption.

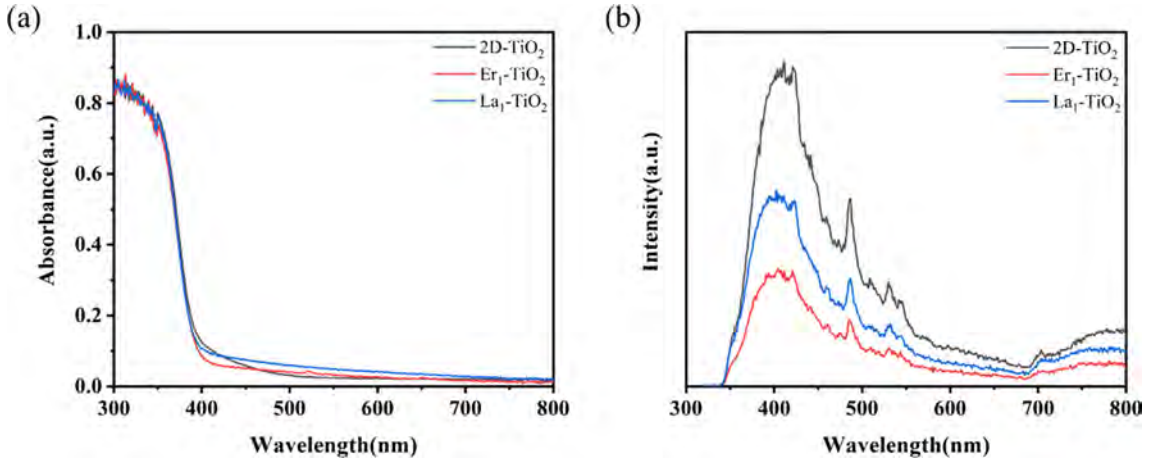

Fig. 5. (a) UV–vis spectra and (b) PL spectra of 2D-TiO_2, Er_1-TiO_2 and La_1-TiO_2.

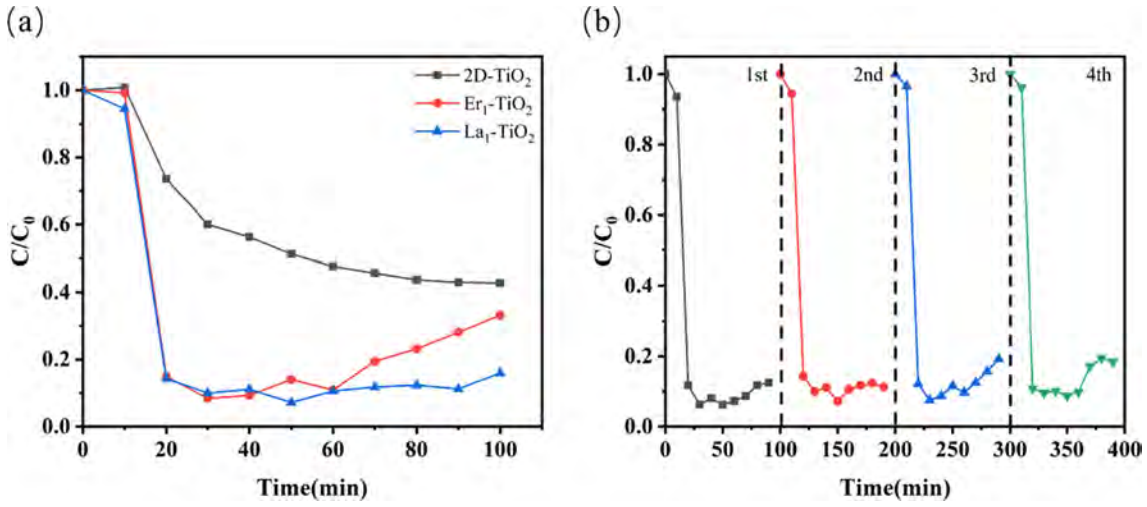

Fig. 6. (a) Photodegradation plots of O-xylene and (b) degradation curve of La_1-TiO_2 for 4 repeated cycles.

3.3. Photocatalytic degradation performance of O-xylene

Dynamic degradation curve reflects photocatalytic degradation performance. As shown in Fig. 6a, the maximal degradation percentage of gaseous O-xylene were 60% and 90% by 2D-TiO_2 and TiO_2 decorated with rare-earth single atoms, respectively. We also compared this work with other studies on RE modified TiO_2 used for photocatalytic degradation of gas phase O-xylene (Table 3). It is worth mentioning that the amount of rare-earth used in Er single atoms decorated TiO_2 was only one fifth of that in Er^{3+} doped TiO_2 when the degradation efficiency was the same. It's observed that the degradation curve of 2D-TiO_2 decreased continuously at first and then remained essentially unchanged after one hour. As for TiO_2 decorated with rare-earth single atoms, removal efficiency reached the maximum in about 30 min and remained unchanged, and then started to decrease after an hour. Due to the synergistic effect of adsorption capacity and charge separation ability, Er_1-TiO_2 and La_1-TiO_2 had similar degradation efficiency at first. However, the decrease rate of Er_1-TiO_2 was faster than that of La_1-TiO_2. There are two reasons that rare-earth single atoms enhanced the photocatalytic degradation performance of 2D-TiO_2. On one hand, the introduction of single atoms which acted as additional adsorption active sites improved the adsorption capacity of O-xylene. On the other hand, charge transfer channel between rare-earth single atom and O atom promoted charge separation and decreased the recombination rate of photo-generated carriers. In order to study the stability of the materials in practice, a cyclic experiment was carried out. As shown in Fig. 6b, La_1-TiO_2 maintained high photocatalytic performance after four circles and exhibited excellent cyclic stability.

Table 3
Comparison of photocatalytic activity of degradation of gas phase O-xylene for the RE modified TiO_2 reported.

Photocatalysts	RE mole ratio	Degradation Efficiency	Reference
Er_1-TiO_2	0.24%	90%	This work
0.5 %Er-TiO_2	0.5%	80%	[27]
2 %Er-TiO_2	2%	85%	[27]
0.5 %Tm-TiO_2	0.5%	90%	[11]

3.4. Proposed mechanism

As the main reactive oxygen species, superoxide radicals ($\cdot O_2^-$) and hydroxyl radicals ($\cdot$OH) play an important role in the photocatalytic reaction process [36]. ESR measurements were carried out to analyze the production of $\cdot O_2^-$ and $\cdot$OH for different samples after illumination. After illumination, the sample produced photo-

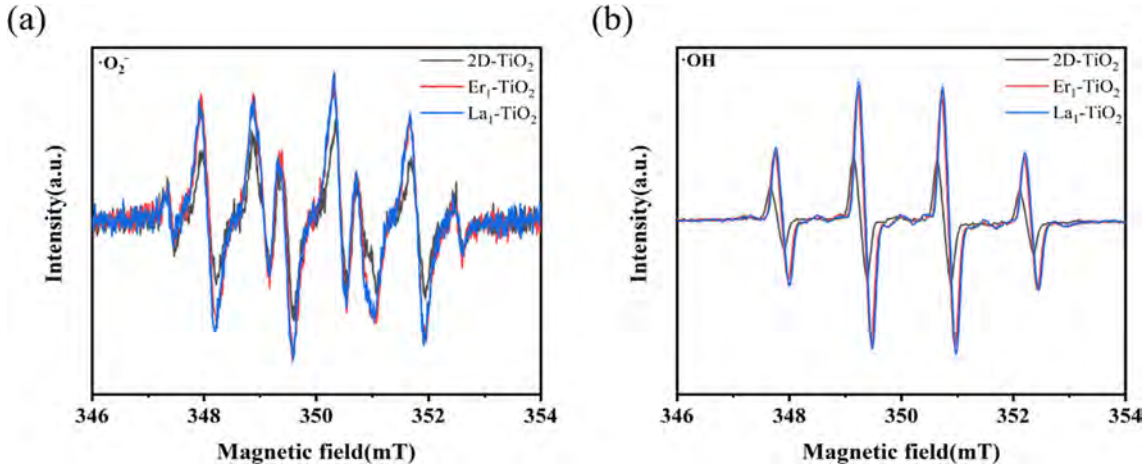

Fig. 7. ESR signals of $\cdot O_2^-$ (a) and $\cdot$OH (b) of TiO_2, Er_1-TiO_2 and La_1-TiO_2.

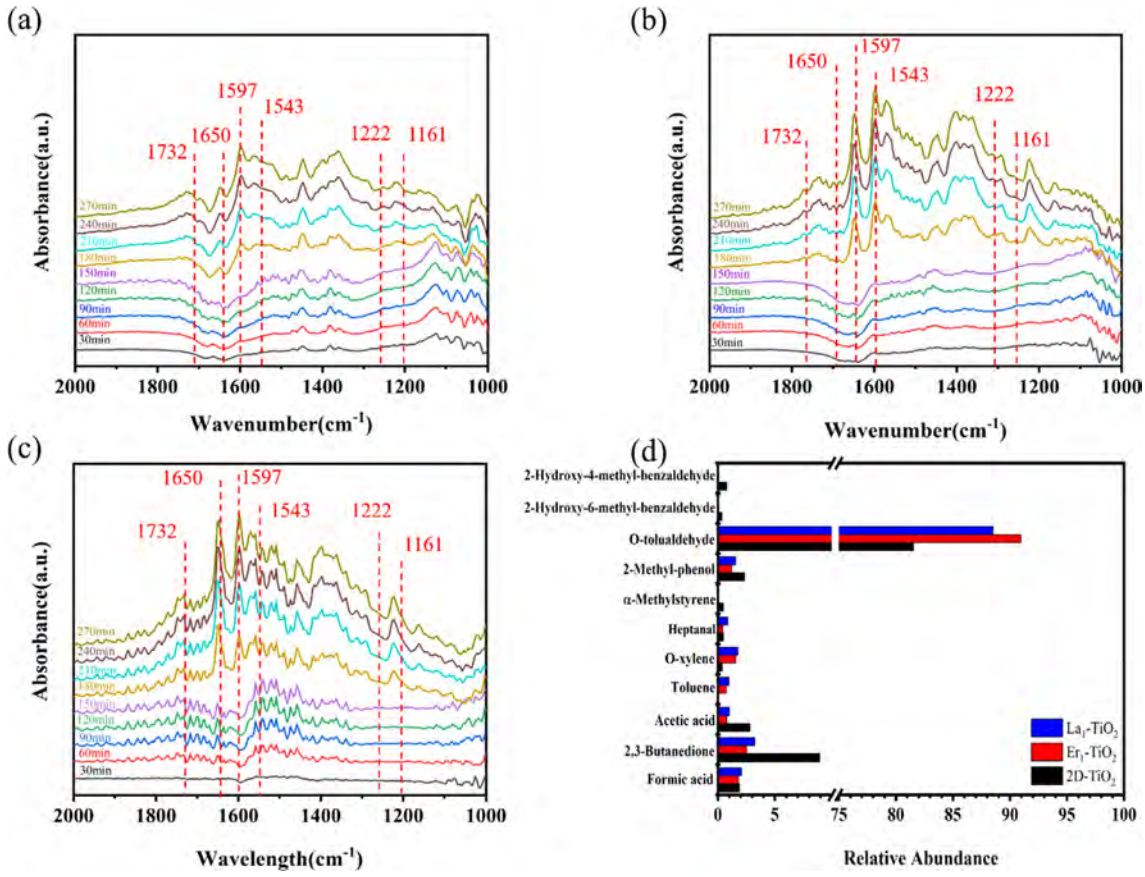

Fig. 8. *In-situ* DRIFTS spectra of dark absorption and photodegradation of O-xylene in the range of 2000–1000 cm^{-1} over the surface of (a) 2D-TiO_2, (b) Er_1-TiO_2 and (c) La_1-TiO_2; (d) the relative abundance of intermediates accumulated on the surface of 2D-TiO_2, Er_1-TiO_2 and La_1-TiO_2.

induced e^- and h^+; then, the e^- attacked O_2 to form $\cdot O_2^-$ while h^+ attacked H_2O to form ·OH; finally, $\cdot O_2^-$ and ·OH reacted with O-xylene and then degraded it. As shown in Fig. 7a and Fig. 7b, the signal of the $\cdot O_2^-$ was stronger than that of the ·OH for different samples, which meant that the $\cdot O_2^-$ may play a more important role during the photocatalytic reaction process. Compared with 2D-TiO_2, TiO_2 decorated with rare-earth single atoms showed stronger signals of both $\cdot O_2^-$ and ·OH in ESR measurements. The presence of single atoms promoted the separation of photo-induced e^- and h^+ to form more $\cdot O_2^-$ and ·OH, which resulted in the improvement of photodegradation performance.

In-situ DRIFTS was applied to monitor the changes of intermediates on the surface of photocatalysts in real-time during the photocatalytic reaction. The representative time resolution spectra of 2D-TiO_2, Er_1-TiO_2 and La_1-TiO_2 were presented in Fig. 8a, Fig. 8b and Fig. 8c, respectively. The characteristic band located at 1732 cm^{-1} could be assigned to the stretch vibration of ν(C=O) of aliphatic compounds (formic acid, acetic acid, butanedione and heptanal) [37,38]. Characteristic bands located at 1650 cm^{-1},1597 cm^{-1} and 1543 cm^{-1} could be associated with the vibration of ν(C=C) of benzene ring [37,39]. The characteristic band located at 1222 cm^{-1} could be assigned to the vibration of ν(C=O) of aromatic aldehydes (o-tolualdehyde) [40]. The characteristic band located at 1161 cm^{-1} could be associated with the vibration of ν(C-OH) of aliphatic compounds (formic acid, acetic acid and butanedione). In contrast with 2D-TiO_2, TiO_2 decorated with rare-earth single atoms had similar characteristic bands and enhanced intensities in the same characteristic bands after 180 min (after irradiation). It meant that more O-xylene were degraded, and more intermediates were formed and accumulated, consistent with the degradation efficiency.

The intermediates were further confirmed by the GC–MS. The types and relative abundance of intermediates observed in different samples were shown in Fig. 8d. O-tolualdehyde was the main intermediate for all samples. However, the relative abundance of Er_1-TiO_2 or La_1-TiO_2 was higher than that of 2D-TiO_2. In general, the methyl of O-xylene was oxidized first during the photocatalytic degradation reaction [41–43]. The higher relative abundance of o-tolualdehyde meant a higher oxidation capacity. In addition, the higher relative abundance of o-tolualdehyde was beneficial for subsequent benzene-ring opening reaction and eventual mineralization. Toxic methyl-phenol formed on 2D-TiO_2 accounted for about 3% of the total intermediates, while the amount of methyl-phenol was reduced on TiO_2 decorated with rare-earth single atoms. Interestingly, α-methylstyrene and hydroxy-methyl-benzaldehyde were detected on 2D-TiO_2, while none of them was detected on Er_1-TiO_2 or La_1-TiO_2. There are two possible reasons for this. On one hand, the presence of more $\cdot O_2^-$ and ·OH in Er_1-TiO_2 or La_1-TiO_2 which readily oxidize o-tolualdehyde into open-ring products without generating α-methylstyrene and hydroxy-methyl-benzaldehyde. On the other hand, the single atoms may direct $\cdot O_2^-$ and ·OH to attack the methyl group instead of the aromatic ring [44], which is also the possible reason for the reduced amount of methyl-phenol when single atoms presented.

Based on the above results, a possible mechanism for photocatalytic degradation of O-xylene was presented in Scheme 1. Compared with pure 2D-TiO_2, TiO_2 decorated with rare-earth single atoms exhibited faster charge separation capacity and stronger

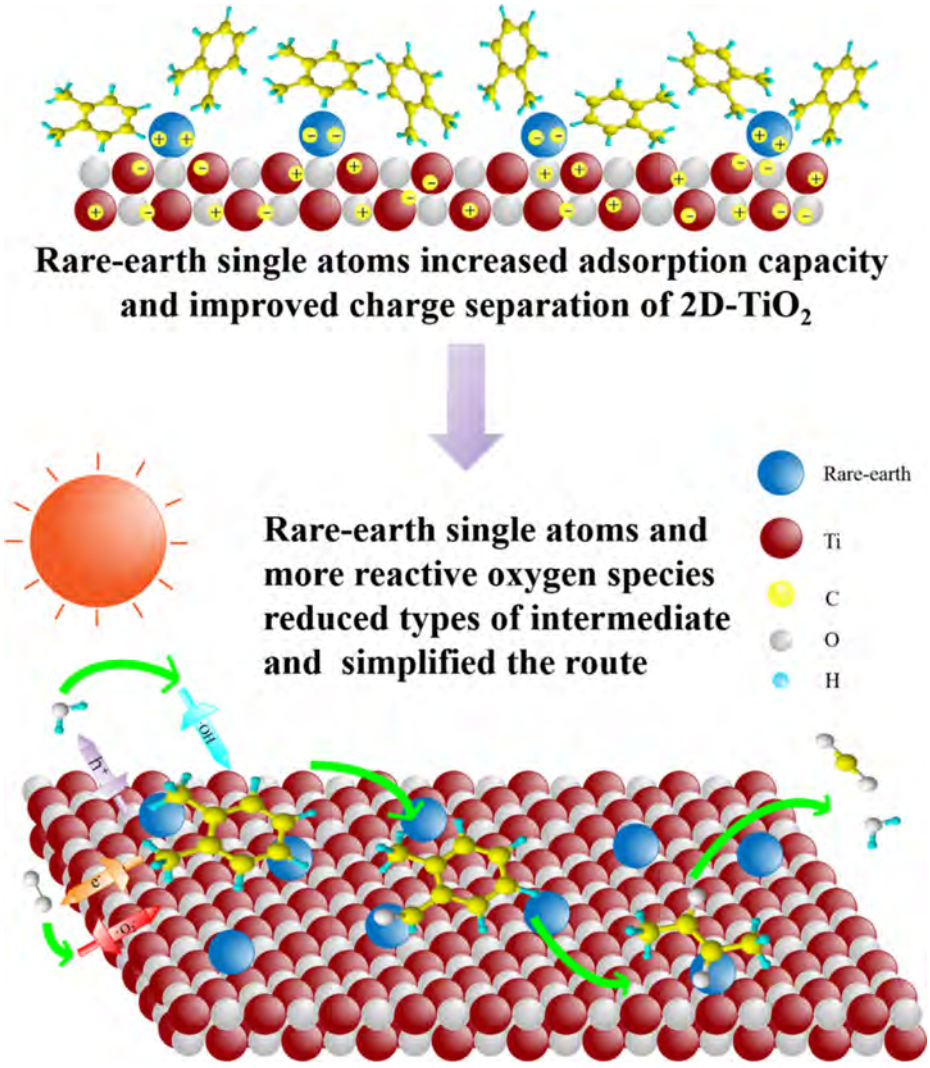

Scheme 1. Schematic diagram of adsorption towards O-xylene and charge separation of TiO_2 decorated with rare-earth single atoms and schematic diagram of photocatalytic degradation process on TiO_2 decorated with rare-earth single atoms.

adsorption capacity. During the whole photocatalytic reaction process, O-xylene molecules were absorbed by the sample under dark at first. Under irradiation, the sample produced photo-induced e^- and h^+. Due to the 2D structure of 2D-TiO_2 nanosheets, the photo-induced e^- and h^+ were transferred to the surface of 2D-TiO_2 easily, then the e^- and h^+ would be promoted to separate by single atoms. After that, the e^- would attack O_2 to form $\cdot O_2^-$ while h^+ would attack H_2O to form ·OH. These two reactive oxygen species would react with O-xylene absorbed to form a series of intermediates and eventually mineralize those intermediates into CO_2 and H_2O. Combining the result of *in-situ* DRIFTS with the result of GC–MS, the possible photocatalytic reaction routes were proposed in Scheme 2. The mineralization process of O-xylene can be summarized as follows: the methyl of O-xylene was oxidized first, and then the oxidation products like o-tolualdehyde underwent a ring-opening reaction to form chain molecules, which finally mineralized into CO_2 and H_2O. It is worth mentioning that the existence of single atoms reduced the types of intermediates and simplified the reaction route. In other words, the existence of single atoms was beneficial to the complete degradation of O-xylene.

4. Conclusion

In summary, TiO_2 decorated with rare-earth single atoms was successfully synthesized by an impregnation-calcination strategy for enhancing photocatalytic degradation efficiency of gaseous O-xylene with remarkable cyclic stability. The enhanced performance of O-xylene removal in TiO_2 decorated with rare-earth single atoms was attributed to the additional active sites formed by coordination between rare-earth single atoms and oxygen atoms, which not only improved the charge separation ability by forming a charge-transfer channel between rare-earth single atom and oxygen atom, but also reduced the adsorption energy to increase the adsorption capacity. In addition, compared with 2D-TiO_2, TiO_2 decorated with rare-earth single atoms reduced the kinds of the intermediates detected and simplified the degradation routes. This study provides a novel TiO_2 decorated with rare-earth single atoms photocatalyst for the effective degradation of O-xylene and provides a strategy to modulate the intermediates and optimize the degradation routes. It is hoped that this work will be helpful to design and application of rare-earth single atoms in photocatalytic degradation VOCs.

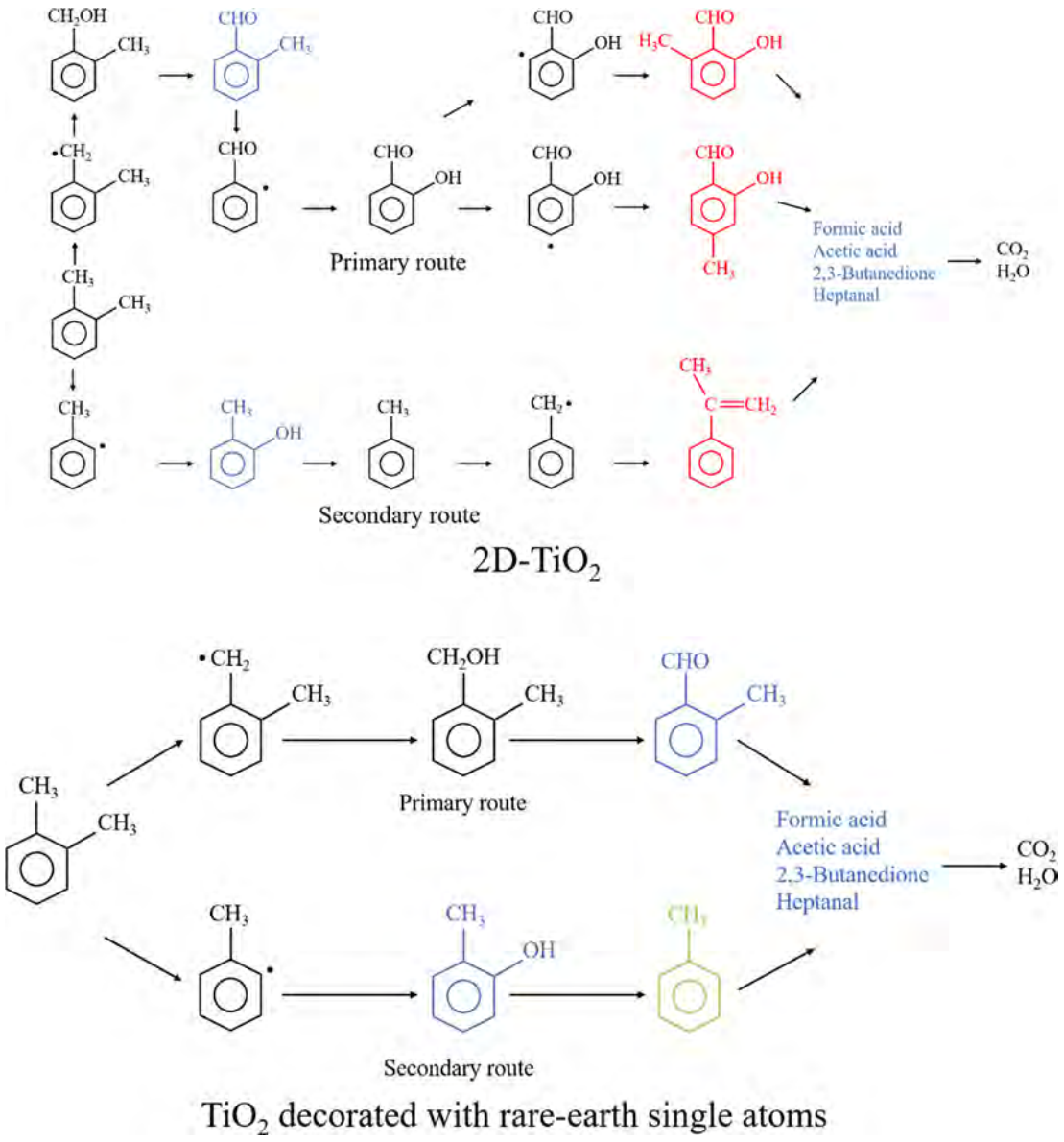

Scheme 2. The possible photocatalytic degradation routes of O-xylene (the blue, red and green products represent the photodegradation intermediates; the red products are peculiar to 2D-TiO_2; the green product is peculiar to TiO_2 decorated with rare-earth single atoms).

CRediT authorship contribution statement

Junfeng Chen: Investigation, Validation, Data curation, Writing – original draft. **Lu Chen:** Methodology, Formal analysis. **Xiao Wang:** Formal analysis, Resources. **Zepeng Rao:** Data curation. **Jing Sun:** Validation, Resources. **Aiying Chen:** Conceptualization, Funding acquisition, Project administration. **Xiaofeng Xie:** Conceptualization, Funding acquisition, Project administration, Writing – review & editing.

Declaration of Competing Interest

The authors declare that they have no known competing financial interests or personal relationships that could have appeared to influence the work reported in this paper.

Acknowledgment

This work was financially supported by the National Key Research and Development Program of China (2016YFA0203000), National Natural Science Foundation of China (51771121), Shanghai Commission of Science and Technology Program (19DZ1202600, 20DZ1204100), the National Natural Science Foundation of China (41907303, 51574205), the State Key Laboratory Director Fund of SICCAS (Y9ZC0102).

References

[1] M. Kampa, E. Castanas, Human health effects of air pollution, Environ. Pollut. 151 (2) (2008) 362–367.
[2] A.H. Mamaghani, F. Haghighat, C.S. Lee, Photocatalytic oxidation technology for indoor environment air purification: The state-of-the-art, Appl. Catal. B: Environ. 203 (2017) 247–269.
[3] S. Wang, H.M. Ang, M.O. Tade, Volatile organic compounds in indoor environment and photocatalytic oxidation: state of the art, Environ. Int. 33 (5) (2007) 694–705.
[4] U. Pöschl, M. Shiraiwa, Multiphase chemistry at the atmosphere-biosphere interface influencing climate and public health in the anthropocene, Chem. Rev. 115 (10) (2015) 4440–4475.
[5] L. Zhong, C.S. Lee, F. Haghighat, Adsorption performance of titanium dioxide (TiO_2) coated air filters for volatile organic compounds, J. Hazard. Mater. 243 (2012) 340–349.

[6] S. Sultana, A. Vandenbroucke, C. Leys, N. De Geyter, R. Morent, Abatement of VOCs with alternate adsorption and plasma-assisted regeneration: a review, Catalysts 5 (2) (2015) 718–746.
[7] H. Wang, W. Yang, P. Tian, J. Zhou, R. Tang, S. Wu, A highly active and anti-coking Pd-Pt/SiO_2 catalyst for catalytic combustion of toluene at low temperature, Appl. Catal. A: Gen. 529 (2017) 60–67.
[8] M.R. Hoffmann, S.T. Martin, W. Choi, D.W. Bahnemann, Environmental applications of semiconductor photocatalysis, Chem. Rev. 95 (1) (1995) 69–96.
[9] Z. Shayegan, C.S. Lee, F. Haghighat, TiO_2 photocatalyst for removal of volatile organic compounds in gas phase - A review, Chem. Eng. J. 334 (2018) 2408–2439.
[10] X. Han, Q. Kuang, M. Jin, Z. Xie, L. Zheng, Synthesis of Titania Nanosheets with a High Percentage of Exposed (001) Facets and Related Photocatalytic Properties, J. Am. Chem. Soc. 131 (9) (2009) 3152–3153.
[11] Z. Rao, G. Shi, Z. Wang, A. Mahmood, X. Xie, J. Sun, Photocatalytic degradation of gaseous VOCs over Tm^{3+}-TiO_2: Revealing the activity enhancement mechanism and different reaction paths, Chem. Eng. J. 395 (2020) 125078.
[12] G. Lu, X. Wang, Y. Wang, G. Shi, X. Xie, J. Sun, Anti-oxidative microstructure design of ultra-stable N-TiO_2 composite for the gaseous photodegradation reactions, Chem. Eng. J. 408 (2021) 127257.
[13] Q. Wu, J. Ye, W. Qiao, Y. Li, J. W. (Hans) Niemantsverdriet, E. Richards, F. Pan, R. Su,, Inhibit The Formation of Toxic Methylphenolic By-products in Photo-decomposition of Formaldehyde-Toluene/Xylene Mixtures by Pd Cocatalyst on TiO_2, Appl. Catal. B: Environ. 291 (2021) 120118.
[14] Wenjiao Lin, Xiaofeng Xie, Xiao Wang, Yan Wang, Doris Segets, Jing Sun, Efficient adsorption and sustainable degradation of gaseous acetaldehyde and o-xylene using rGO-TiO_2 photocatalyst, Chem. Eng. J. 349 (2018) 708–718.
[15] Xueping Dai, Guanhong Lu, Yidan Hu, Xiaofeng Xie, Xiao Wang, Jing Sun, Reversible redox behavior of Fe_2O_3/TiO_2 composites in the gaseous photodegradation process, Ceram. Int. 45 (10) (2019) 13187–13192.
[16] J. Feng, H. Huang, T. Fang, X. Wang, S. Yan, W. Luo, T. Yu, Y. Zhao, Z. Li, Z. Zou, Defect Engineering in Semiconductors: Manipulating Nonstoichiometric Defects and Understanding Their Impact in Oxynitrides for Solar Energy Conversion, Adv. Funct. Mater. 29 (2019) 1808389.
[17] Shufang Ji, Yuanjun Chen, Xiaolu Wang, Zedong Zhang, Dingsheng Wang, Yadong Li, Chemical Synthesis of Single Atomic Site Catalysts, Chem. Rev. 120 (21) (2020) 11900–11955.
[18] B. Qiao, A. Wang, X. Yang, L.F. Allard, Z. Jiang, Y. Cui, J. Liu, J. Li, T. Zhang, Single-atom catalysis of CO oxidation using Pt1/FeOx, Nat. Chem. 3 (2011) 634–641.
[19] J. Wan, W. Chen, C. Jia, L. Zheng, J. Dong, X. Zheng, Y. Wang, W. Yan, C. Chen, Q. Peng, D. Wang, Y. Li, Defect Effects on TiO2 Nanosheets: Stabilizing Single Atomic Site Au and Promoting Catalytic Properties, Adv. Mater. 30 (2018) 1705369.
[20] J. Li, D. Yi, F. Zhan, B. Zhou, D. Gao, D. Guo, S. Liu, X. Wang, J. Yao, Monolayered Ru_1/TiO_2 nanosheet enables efficient visible-light-driven hydrogen evolution, Appl. Catal. B: Environ. 271 (2020) 118925.
[21] Zupeng Chen, Sergey Pronkin, Tim-Patrick Fellinger, Kamalakannan Kailasam, Gianvito Vilé, Davide Albani, Frank Krumeich, Rowan Leary, Jon Barnard, John Meurig Thomas, Javier Pérez-Ramírez, Markus Antonietti, Dariya Dontsova, Merging Single-Atom-Dispersed Silver and Carbon Nitride to a Joint Electronic System via Copolymerization with Silver Tricyanomethanide, ACS Nano 10 (3) (2016) 3166–3175.
[22] Z. Hu, X. Li, S. Zhang, Q. Li, J. Fan, X. Qu, K. Lv, Fe_1/TiO_2 Hollow Microspheres: Fe and Ti Dual Active Sites Boosting the Photocatalytic Oxidation of NO, Small 16 (2020) 2004583.
[23] X. Wu, S. Zuo, M. Qiu, Y. Li, Y. Zhang, P. An, J. Zhang, H. Zhang, J. Zhang, Atomically Defined Co on Two-Dimensional TiO_2 Nanosheet for Photocatalytic Hydrogen Evolution, Chem. Eng. J. 420 (2021) 127681.
[24] Mu Xiao, Lei Zhang, Bin Luo, Miaoqiang Lyu, Zhiliang Wang, Hengming Huang, Songcan Wang, Aijun Du, Lianzhou Wang, Molten-Salt-Mediated Synthesis of an Atomic Nickel Co-catalyst on TiO_2 for Improved Photocatalytic H_2 Evolution, Angew. Chem. Int. Ed. 59 (18) (2020) 7230–7234.
[25] Byoung-Hoon Lee, Sunghak Park, Minho Kim, Arun K. Sinha, Seong Chan Lee, Euiyeon Jung, Woo Je Chang, Kug-Seung Lee, Jeong Hyun Kim, Sung-Pyo Cho, Hyungjun Kim, Ki Tae Nam, Taeghwan Hyeon, Reversible and cooperative photoactivation of single-atom Cu/TiO_2 photocatalysts, Nat. Mater. 18 (6) (2019) 620–626.
[26] J. Castañeda-Contreras, V.F. Marañón-Ruiz, R. Chiu-Zárate, H. Pérez-Ladrón de Guevara, R. Rodriguez, C. Michel-Uribe, Photocatalytic Activity of Erbium-Doped TiO_2 Nanoparticles Im-mobilized in Macro-Porous Silica Films, Mater. Res. Bull. 47 (2) (2012) 290–295.
[27] Zepeng Rao, Xiaofeng Xie, Xiao Wang, Asad Mahmood, Shengrui Tong, Maofa Ge, Jing Sun, Defect Chemistry of Er^{3+}-Doped TiO_2 and Its Photocatalytic Activity for the Degradation of Flowing Gas-Phase VOCs, J. Phys. Chem. C 123 (19) (2019) 12321–12334.
[28] Jieyuan Liu, Xue Kong, Lirong Zheng, Xu Guo, Xiaofang Liu, Jianglan Shui, Rare Earth Single-Atom Catalysts for Nitrogen and Carbon Dioxide Reduction, ACS Nano 14 (1) (2020) 1093–1101.
[29] Shufang Ji, Yang Qu, Tao Wang, Yuanjun Chen, Guofeng Wang, Xue Li, Juncai Dong, QiuYu Chen, Wanying Zhang, Zedong Zhang, Shiyou Liang, Rong Yu, Yu Wang, Dingsheng Wang, Yadong Li, Rare-Earth Single Erbium Atoms for Enhanced Photocatalytic CO_2 Reduction, Angew. Chem. Int. Ed. 59 (26) (2020) 10651–10657.
[30] Peng Chen, Ben Lei, Xing'an Dong, Hong Wang, Jianping Sheng, Wen Cui, Jieyuan Li, Yanjuan Sun, Zhiming Wang, Fan Dong, Rare-Earth Single-Atom La-N Charge-Transfer Bridge on Carbon Nitride for Highly Efficient and Selective Photocatalytic CO_2 Reduction, ACS Nano 14 (11) (2020) 15841–15852.
[31] Jingsheng Cai, Jiali Shen, Xinnan Zhang, Yun Hau Ng, Jianying Huang, Wenxi Guo, Changjian Lin, Yuekun Lai, Light-Driven Sustainable Hydrogen Production Utilizing TiO_2 Nanostructures: A Review, Small Methods. 3 (1) (2019) 1800184, https://doi.org/10.1002/smtd.v3.110.1002/smtd.201800184.
[32] Toshiaki Ohsaka, Fujio Izumi, Yoshinori Fujiki, Raman-spectrum of anatase TiO_2, J. Raman Spectrosc. 7 (6) (1978) 321–324.
[33] Q. Zeng, X. Wang, X. Xie, G. Lu, Y. Wang, S.C. Lee, J. Sun, TiO_2/TaS_2 with superior charge separation and adsorptive capacity to the photodegradation of gaseous acetaldehyde, Chem. Eng. J. 379 (2020) 122395.
[34] Z. Zhang, Y. Zhu, H. Asakura, B. Zhang, J. Zhang, M. Zhou, Y. Han, Tsunehiro Tanaka, Aiqin Wang, Tao Zhang, Ning Yan, Thermally stable single atom Pt/m-Al_2O_3 for selective hydrogenation and CO oxidation, Nat. Commun. 8 (2017) 16100.
[35] Z. Wang, A. Mahmood, X. Xie, X. Wang, H. Qiu, J. Sun, Surface adsorption configurations of H_3PO_4 modified TiO_2 and its influence on the photodegradation intermediates of gaseous o-xylene, Chem. Eng. J. 393 (2020) 124723.
[36] Yoshio Nosaka, Atsuko Y. Nosaka, Generation and detection of reactive oxygen species in photo-catalysis, Chem. Rev. 117 (17) (2017) 11302–11336.
[37] M. Lai, J. Zhao, Q. Chen, S. Feng, Y. Bai, Y. Li, C. Wang, Photocatalytic toluene degradation over Bi-decorated TiO_2: promoted O_2 supply to catalyst's surface by metallic Bi, Catal. Today 335 (2019) 372–380.
[38] X. Li, Z. Zhu, Q. Zhao, S. Liu, FT-IR study of the photocatalytic degradation of gaseous toluene over UV-irradiated TiO_2 micro-balls: enhanced performance by hydrothermal treatment in alkaline solution, Appl. Surf. Sci. 257 (2011) 4709–4714.
[39] M.D. Hernández-Alonso, I. Tejedor-Tejedor, J.M. Coronado, M.A. Anderson, Operando FTIR study of the photocatalytic oxidation of methylcyclohexane and toluene in air over TiO_2-ZrO_2 thin films: influence of the aromaticity of the target molecule on deactivation, Appl. Catal. B: Environ. 101 (2011) 283–293.
[40] Jieyuan Li, Xing'an Dong, Guan Zhang, Wen Cui, Wanglai Cen, Zhongbiao Wu, S. C. Lee, Fan Dong, Probing ring-opening pathways for efficient photocatalytic toluene decomposition, J. Mater. Chem. A 7 (7) (2019) 3366–3374.
[41] M. Sleiman, P. Conchon, C. Ferronato, J.M. Chovelon, Photocatalytic oxidation of toluene at indoor air levels (ppbv): towards a better assessment of conversion, reaction intermediates and mineralization, Appl. Catal. B: Environ. 86 (2009) 159–165.
[42] Yu Huang, Steven Ho, Yanfeng Lu, Ruiyuan Niu, Lifeng Xu, Junji Cao, Shuncheng Lee, Removal of indoor volatile organic compounds via photocatalytic oxidation: a short review and prospect, Molecules 21 (1) (2016) 56, https://doi.org/10.3390/molecules21010056.
[43] P. Chen, W. Cui, H. Wang, X. Dong, J. Li, Y. Sun, Y. Zhou, Y. Zhang, F. Dong, The importance of intermediates ring-opening in preventing photo-catalyst deactivation during toluene decomposition, Appl. Catal. B: Environ. 272 (2020) 118977.
[44] Q. Wu, J. Ye, W. Qiao, Y. Li, J.W. (Hans) Niemantsverdriet, E. Richards, F. Pan, R. Su,, Inhibit the formation of toxic methylphenolic by-products in photo-decomposition of formaldehyde-toluene/xylene mixtures by Pd cocatalyst on TiO_2, Appl. Catal. B: Environ. 291 (2021) 120118.